Article

Cell Reports

Subtle Changes in the Levels of BCL-2 Proteins Cause Severe Craniofacial Abnormalities

Graphical Abstract

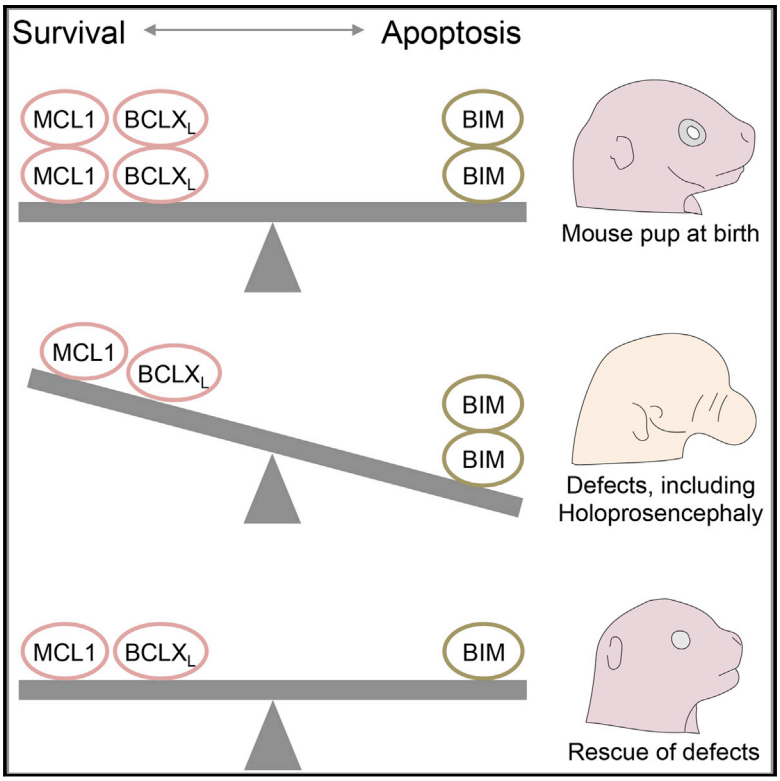

Highlights

- Control of embryonic cell survival by BCL-2 family proteins is finely balanced
- Combined loss of single alleles of *Mcl-1* and *Bcl-x* causes craniofacial defects
- Loss of one allele of *Bim* restores normal development to *Mcl-1*$^{+/-}$;*Bcl-x*$^{+/-}$ pups

Authors

Stephanie Grabow, Andrew J. Kueh, Francine Ke, ..., Lachlan Whitehead, Anne K. Voss, Andreas Strasser

Correspondence

sgrabow@merrimack.com (S.G.), avoss@wehi.edu.au (A.K.V.), strasser@wehi.edu.au (A.S.)

In Brief

Grabow et al. find that combined loss of single alleles of pro-survival *Mcl-1* and *Bcl-x* causes craniofacial defects, including holoprosencephaly, a severe birth defect. Normal development is restored by concomitant loss of a single allele of pro-apoptotic *Bim*, revealing that cell survival and cell death during embryogenesis are finely balanced.

Grabow et al., 2018, Cell Reports *24*, 3285–3295
September 18, 2018
https://doi.org/10.1016/j.celrep.2018.08.048

CellPress

Cell Reports
Article

Subtle Changes in the Levels of BCL-2 Proteins Cause Severe Craniofacial Abnormalities

Stephanie Grabow,[1,2,6,10,*] Andrew J. Kueh,[1,2,10] Francine Ke,[1,2] Hannah K. Vanyai,[1,2,7] Bilal N. Sheikh,[1,2,8] Michael A. Dengler,[1,2] William Chiang,[1,2] Samantha Eccles,[1] Ian M. Smyth,[3,4] Lynelle K. Jones,[3,4] Frederic J. de Sauvage,[5] Mark Scott,[1,9] Lachlan Whitehead,[1,2] Anne K. Voss,[1,2,11,12,*] and Andreas Strasser[1,2,11,*]

[1]The Walter and Eliza Hall Institute of Medical Research, Melbourne, VIC 3052, Australia
[2]Department of Medical Biology, The University of Melbourne, Melbourne, VIC 3052, Australia
[3]Development and Stem Cells Program, Monash Biomedicine Discovery Institute, Monash University, Melbourne, VIC 3800, Australia
[4]Department of Anatomy and Developmental Biology and Department of Biochemistry and Molecular Biology, Monash University, Melbourne, VIC 3800, Australia
[5]Department of Molecular Oncology, Genentech, South San Francisco, CA 94080, USA
[6]Present address: Merrimack Pharmaceuticals, 1 Kendall Square, Cambridge, MA 02139, USA
[7]Present address: The Francis Crick Institute, Kings Cross, London NW1 1AT, UK
[8]Present address: Max Planck Institute of Immunology and Epigenetics, 79108 Freiburg, Baden-Wuerttemberg, Germany
[9]Present address: Institute of Molecular Bioscience, University of Queensland, Lucia, QLD 4072, Australia
[10]These authors contributed equally
[11]Senior author
[12]Lead Contact
*Correspondence: sgrabow@merrimack.com (S.G.), avoss@wehi.edu.au (A.K.V.), strasser@wehi.edu.au (A.S.)
https://doi.org/10.1016/j.celrep.2018.08.048

SUMMARY

Apoptotic cell death removes unwanted cells and is regulated by interactions between pro-survival and pro-apoptotic members of the BCL-2 protein family. The regulation of apoptosis is thought to be crucial for normal embryonic development. Accordingly, complete loss of pro-survival MCL-1 or BCL-XL (BCL2L1) causes embryonic lethality. However, it is not known whether minor reductions in pro-survival proteins could cause developmental abnormalities. We explored the rate-limiting roles of MCL-1 and BCL-XL in development and show that combined loss of single alleles of *Mcl-1* and *Bcl-x* causes neonatal lethality. *Mcl-1*$^{+/-}$*;Bcl-x*$^{+/-}$ mice display craniofacial anomalies, but additional loss of a single allele of pro-apoptotic *Bim* (*Bcl2l11*) restores normal development. These findings demonstrate that the control of cell survival during embryogenesis is finely balanced and suggest that some human craniofacial defects, for which causes are currently unknown, may be due to subtle imbalances between pro-survival and pro-apoptotic BCL-2 family members.

INTRODUCTION

Craniofacial anomalies are among the most common human birth defects and are often associated with fetal or infant death, as well as with intellectual and/or physical disability. Of these defects, holoprosencephaly (HPE) is the most common developmental anomaly of the forebrain. It is characterized by a complete or partial failure of division of the single midline prosencephalon into the bilateral hemispheres, and this is typically associated with midline facial defects (Petryk et al., 2015). Holoprosencephaly has an incidence of 1 in 16,000 live births (Roach et al., 1975) and 1 in 250 spontaneous abortions in humans (Matsunaga and Shiota, 1977). Although holoprosencephaly is known for its association with mutations in the sonic hedgehog (SHH) (Belloni et al., 1996; Chiang et al., 1996; Roessler et al., 1996) and nodal signaling pathways (Chu et al., 2005; Nomura and Li, 1998) or defects in genes, such as *ZIC2* (Brown et al., 1998), *SIX3* (Wallis et al., 1999), *SOX9* (Wright et al., 1995), and *TGIF* (Gripp et al., 2000), known genetic mutations explain only ~30% of clinical cases (Geng and Oliver, 2009). Intriguingly, within the same kindred, it has been found that carriers of the same heterozygous mutations can be phenotypically normal or present with severely abnormal craniofacial features, respectively, suggesting the involvement of presently unknown modifying mechanisms (Geng and Oliver, 2009).

The intrinsic (also called BCL-2-regulated, mitochondrial, or stress-induced) apoptotic pathway is thought to be critical for shaping the developing embryo (Kulesa et al., 2004) and therefore constitutes a candidate mechanism that may affect developmental outcomes. The intrinsic apoptosis pathway is regulated by the opposing actions of pro-survival and pro-apoptotic members of the BCL-2 protein family. The family contains five pro-survival members—BCL-2, BCL-XL, BCL-W, MCL-1, and A1/BFL1—and two pro-apoptotic subgroups. The pro-apoptotic BH3-only proteins (BIM, PUMA, BID, BIK, BAD, BMF, NOXA, and HRK) are critical for the initiation of apoptosis signaling, whereas the pro-apoptotic BAX/BAK proteins (also including BOK) are essential for the effector phase of apoptosis (Carpio et al., 2016; Chipuk and Green, 2008; Czabotar et al., 2014; Ke et al., 2012, 2018; Llambi et al., 2016; Youle and Strasser, 2008). In healthy cells, the BAX/BAK cell death effectors are kept in check by the pro-survival BCL-2 family members. In response to programmed cell death stimuli, BH3-only proteins are transcriptionally and/or post-transcriptionally induced. They

bind and inhibit the pro-survival BCL-2-like proteins, thereby unleashing BAX/BAK to kill cells, although some BH3-only proteins may also directly activate BAX/BAK (Chipuk and Green, 2008; Czabotar et al., 2014; Youle and Strasser, 2008).

The pro-survival BCL-2 family members are essential for cell survival, including in embryonic development, exhibiting cell type-specific as well as overlapping roles. Complete loss of the pro-survival protein MCL-1 causes embryonic lethality at the blastocyst stage prior to implantation (embryonic day 3.5 [E3.5]) (Rinkenberger et al., 2000). BCL-XL-deficient embryos die around E13.5 because of abnormally increased apoptosis of erythroid progenitors and certain neuronal populations (Motoyama et al., 1995). *Mcl1*$^{+/-}$ and *Bclx*$^{+/-}$ heterozygous mice are largely normal (Motoyama et al., 1995; Rinkenberger et al., 2000), although the former have a significant, albeit minor, decrease in B lymphocytes that is associated with a ~40% reduction in MCL-1 protein (Brinkmann et al., 2017). We hypothesized that MCL-1 and BCL-XL might have overlapping, cell survival-essential functions in embryonic development. Here we show that combined loss of single alleles of *Mcl-1* and *Bcl-x* is sufficient to disrupt normal embryonic development and that other pro-survival proteins cannot compensate for the subtle reduction in MCL-1 and BCL-XL. *Mcl-1*$^{+/-}$;*Bcl-x*$^{+/-}$ embryos display a range of craniofacial anomalies, including cases of holoprosencephaly. Remarkably, these defects were completely corrected by loss of just one allele of the pro-apoptotic BH3-only protein-encoding gene *Bim*. We conclude that a major function of MCL-1 and BCL-XL during embryonic development must be to keep the pro-apoptotic BH3-only protein BIM in check. These findings demonstrate that a surprisingly tight balance between these three BCL-2 family members controls apoptotic cell death in the embryo, particularly in craniofacial morphogenesis.

RESULTS

Mcl-1$^{+/-}$ Mice Display a Minor Increase in the Incidence of Palpebral Fissure Defects and Hydrocephalus

Of all knockout studies of pro-survival BCL-2 family members, the *Mcl-1*$^{-/-}$ and *Bcl-x*$^{-/-}$ mice showed the most dramatic defects (Motoyama et al., 1995; Rinkenberger et al., 2000). We therefore prioritized MCL-1 and BCL-XL for investigation of possible overlapping functions in embryogenesis and explored this genetically by examining doubly heterozygous, *Mcl-1*$^{+/-}$;*Bcl-x*$^{+/-}$ mice.

First, we established whether loss of one allele of either *Mcl-1* or *Bcl-x* has any consequences on normal mouse development. Intercrosses of either *Mcl-1*$^{+/-}$ or *Bcl-x*$^{+/-}$ mice with wild-type (WT) animals produced viable *Mcl-1*$^{+/-}$ or *Bcl-x*$^{+/-}$ offspring. The frequency of *Bcl-x*$^{+/-}$ heterozygotes at weaning was reduced by ~50% compared with WT (83 *Bcl-x*$^{+/-}$ versus 181 WT, $p < 0.0005$, Fisher's exact test), indicating a haploinsufficient lethality with ~50% penetrance that has not been reported so far but is not the subject of this study. Although the majority of the *Mcl-1*$^{+/-}$ and the surviving *Bcl-x*$^{+/-}$ pups had a normal lifespan, some *Mcl-1*$^{+/-}$ offspring exhibited an increased incidence of hydrocephalus, evident prior to weaning, with concomitant one-sided narrow palpebral fissures compared with WT littermates (4.8% *Mcl-1*$^{+/-}$ versus 0.9% WT, $p = 0.027$, Fisher's exact test; Figure 1A). Other developmental anomalies, such as malocclusion, occurred at similar frequencies in *Mcl-1*$^{+/-}$ and WT mice (1.7% *Mcl-1*$^{+/-}$ versus 2.1% WT, $p = 1$; Figure 1A). Hydrocephalus (1.2% *Bcl-x*$^{+/-}$ versus 0% WT, $p = 0.555$; Figure 1A) and malocclusion (1.2% *Bcl-x*$^{+/-}$ versus 1.7% WT, $p = 1$; Figure 1A) occurred with similar frequency in *Bcl-x*$^{+/-}$ mice and their WT littermates.

As a prerequisite for overlapping function, it would be expected that *Mcl-1* and *Bcl-x* have overlapping gene expression patterns during embryogenesis. *In situ* hybridization revealed prominent expression of *Mcl-1* mRNA in the maxillary and mandibular component of the first pharyngeal arch in E9.5 WT embryos, whereas *Bcl-x* mRNA was found to be highly expressed in the first and second pharyngeal pouch of E9.5 embryos. Both *Mcl-1* and *Bcl-x* mRNA were detected throughout the fore-, mid-, and hindbrain regions, along the neural tube, and in the optic as well as the otic vesicles at E9.5 (Figure 1B). *Mcl-1* and *Bcl-x* mRNA were present at lower levels throughout the E9.5 embryos. These results demonstrate that *Mcl-1* and *Bcl-x* have substantial overlap in their expression during embryogenesis and reveal that morphogenesis can occur normally in the absence of one allele of either of these genes.

Combined Loss of One Allele of *Mcl-1* and *Bcl-x* Causes a Loss of Offspring at Birth because of Severe Developmental Anomalies

We crossed *Mcl-1*$^{+/-}$ with *Bcl-x*$^{+/-}$ mice to determine the functional overlap of these pro-survival proteins. At weaning *Mcl-1*$^{+/-}$;*Bcl-x*$^{+/-}$ mice were present at a frequency of only 3.4% (cf. 25% expected, $p = 0.002$; Figure 1C). A reduction in the litter size was noted in *Mcl-1*$^{+/-}$-by-*Bcl-x*$^{+/-}$ matings already at birth compared with WT intercrosses. The losses at birth and at weaning were similar, suggesting that the missing offspring from *Mcl-1*$^{+/-}$-by-*Bcl-x*$^{+/-}$ matings died before or at birth (Figure 1D).

Timed matings were established to determine the time and cause of death of *Mcl-1*$^{+/-}$;*Bcl-x*$^{+/-}$ mice. At E19.5, *Mcl-1*$^{+/-}$-by-*Bcl-x*$^{+/-}$ matings produced fewer single- and double-heterozygous pups such that the overall distribution of genotypes differed significantly from the expected Mendelian ratio ($p = 0.019$; Figure 2A). Specifically, *Mcl-1*$^{+/-}$;*Bcl-x*$^{+/-}$ pups were present at a modestly reduced frequency (17%) compared with expectation (25%) ($p = 0.034$).

The body weight of the *Mcl-1*$^{+/-}$;*Bcl-x*$^{+/-}$ double-heterozygous pups was substantially decreased (24%; 0.979 ± 0.032 g [n = 38]) compared with the WT ($p < 0.0005$; 1.286 ± 0.017 g [n = 82]), *Mcl-1*$^{+/-}$ (19%; $p < 0.0005$; 1.216 ± 0.015 g [n = 57]), and *Bcl-x*$^{+/-}$ (20%; $p < 0.0005$; 1.223 ± 0.020 g [n = 55]; Figure 2B) littermates and compared with E19.5 pups of WT-by-WT crosses (1.273 ± 0.0134 g [n = 52]).

The *Mcl-1*$^{+/-}$;*Bcl-x*$^{+/-}$ pups exhibited a range of craniofacial anomalies with varying severity (Figure 2C), including hydrocephalus, micrognathia (small jaw), microphthalmia (small eyeballs), or anophthalmia (lack of one or both eyes) and holoprosencephaly. About 10% of *Mcl-1*$^{+/-}$;*Bcl-x*$^{+/-}$ pups developed cyclopia (4 of 41). Furthermore, ~7% presented with exencephaly (3 of 41), ~50% with unilateral or bilateral anophthalmia or microphthalmia (21 of 41), and 44% with overt palate defects (18 of 41), which included a cleft palate. Only 22% of *Mcl-1*$^{+/-}$;*Bcl-x*$^{+/-}$ pups had developed normally.

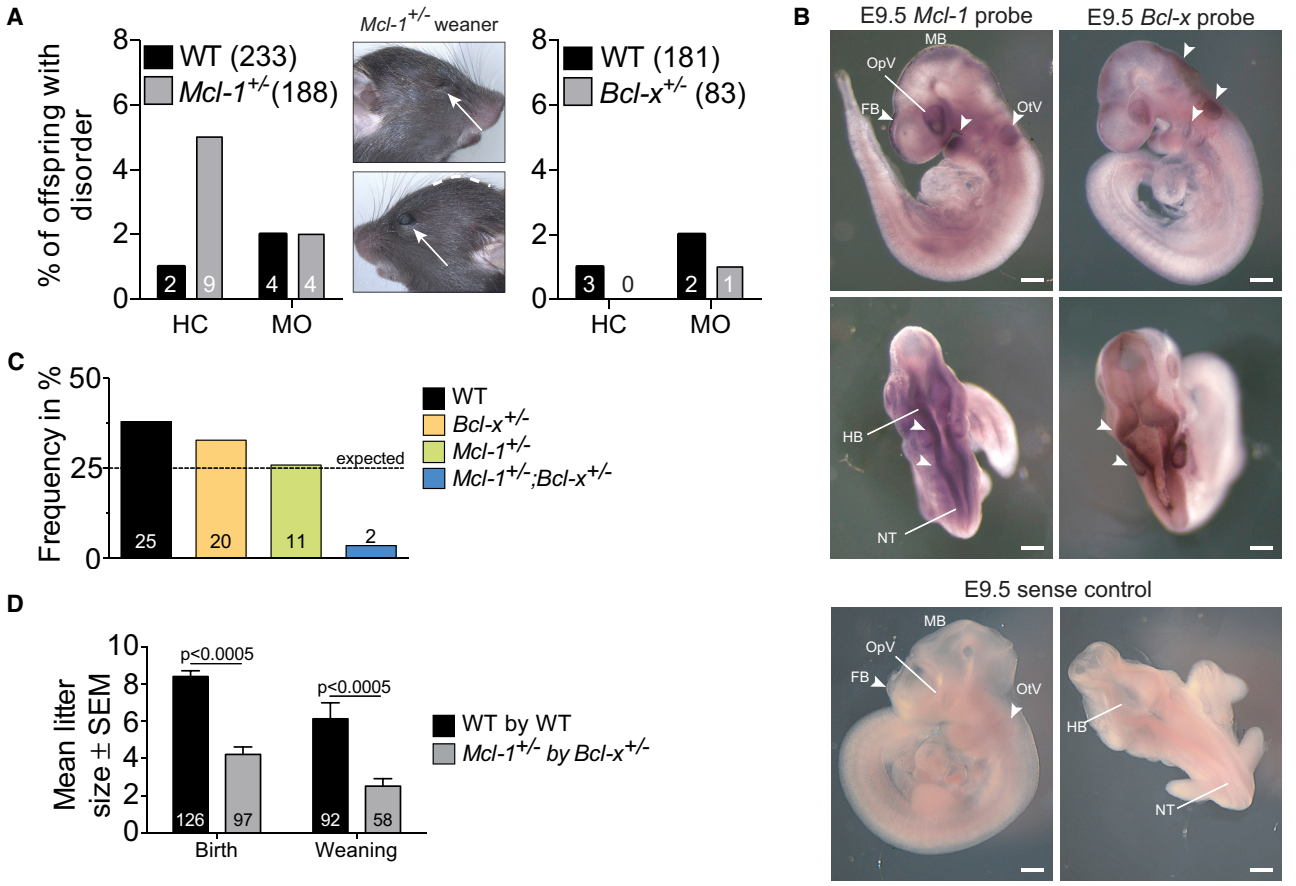

Figure 1. Expression of *Mcl-1* and *Bcl-x* mRNA and Lethality of *Mcl-1*$^{+/-}$;*Bcl-x*$^{+/-}$ Double-Heterozygous Mice

(A) Percentages of *Mcl-1*$^{+/-}$ or *Bcl-x*$^{+/-}$ offspring with hydrocephalus (HC) and/or malocclusion (MO) compared with their WT littermates. Depiction of a *Mcl-1*$^{+/-}$ mouse at 3 weeks of age with right-sided narrow palpebral fissure (cf. normal left eye; arrows) and hydrocephalus (note dome-shaped head; dashed line).

(B) *In situ* hybridization to detect *Mcl-1* or *Bcl-x* mRNA in E9.5 WT embryos, using a *Bax* sense probe as a negative control. Scale bars, 170 μm (top and middle) and 270 μm (bottom).

(C) Frequency of mice of the indicated genotypes at 3 weeks of age.

(D) Mean ± SEM offspring number per litter at birth and weaning (3 weeks of age) of *Mcl-1*$^{+/-}$-by-*Bcl-x*$^{+/-}$ matings compared with WT intercrosses.

n = numbers of mice examined are displayed within the individual bars. FB, forebrain; HB, hindbrain; MB, midbrain; NT, neural tube; OpV, optic vesicle; OtV, otic vesicle.

A quarter of E19.5 *Mcl-1*$^{+/-}$ pups displayed eye defects (14 of 57), and 7% also displayed palate defects (4 of 57). Approximately 7% of *Bcl-x*$^{+/-}$ (4 of 55) but only 1% of WT offspring (1 of 90) showed eye defects alone, and 4% of *Bcl-x*$^{+/-}$ pups presented with combined eye and palate defects (2 of 55; Figure 2D).

Both holoprosencephaly and cyclopia can be caused by a failure of midline formation (Hayhurst and McConnell, 2003). These findings reveal that embryogenesis, particularly craniofacial development, is prominently affected by only subtle reductions in both MCL-1 and BCL-XL.

Combined Loss of One Allele of *Mcl-1* and *Bcl-2* or One Allele of *Bcl-x* and *Bcl-2* Does Not Cause Developmental Abnormalities

To assess whether similar functional redundancy existed between other pairs of pro-survival BCL-2 family members, we crossed *Mcl-1*$^{+/-}$ with *Bcl-2*$^{+/-}$ mice (Figure 3A) and *Bcl-x*$^{+/-}$ with *Bcl-2*$^{+/-}$ mice (Figure 3B) and analyzed their offspring at E19.5. Although most (89%) *Bcl-2*$^{+/-}$ offspring were normal in both mating strategies, 11% of *Bcl-2*$^{+/-}$ pups developed eye defects similarly to the *Mcl-1*$^{+/-}$ pups. No anomalies were observed in the *Bcl-x*$^{+/-}$ offspring arising from the *Bcl-x*$^{+/-}$-by-*Bcl-2*$^{+/-}$ matings (Figure 3A; cf. the larger number of *Bcl-x*$^{+/-}$ offspring with a low percentage of anomalies in the *Mcl-1*$^{+/-}$-by-*Bcl-x*$^{+/-}$ matings [Figure 2D]). *Mcl-1*$^{+/-}$ offspring showed similar frequencies of eye (15%) and palate (5%) defects as observed in the *Mcl-1*$^{+/-}$-by-*Bcl-x*$^{+/-}$ matings. Only 1 of 25 *Bcl-2*$^{+/-}$ offspring showed eye anomalies, and only 4 of 34 and 1 of 34 *Mcl-1*$^{+/-}$;*Bcl-2*$^{+/-}$ pups had eye or combined eye and palate defects, respectively. Of note, most *Mcl-1*$^{+/-}$;*Bcl-2*$^{+/-}$ (n = 9) and *Bcl-x*$^{+/-}$;*Bcl-2*$^{+/-}$ (n = 17) offspring survived into late adulthood (>300 days) without any further obvious anomalies. Because *Mcl-1* heterozygosity and *Bcl-x* heterozygosity displayed genetic interaction with

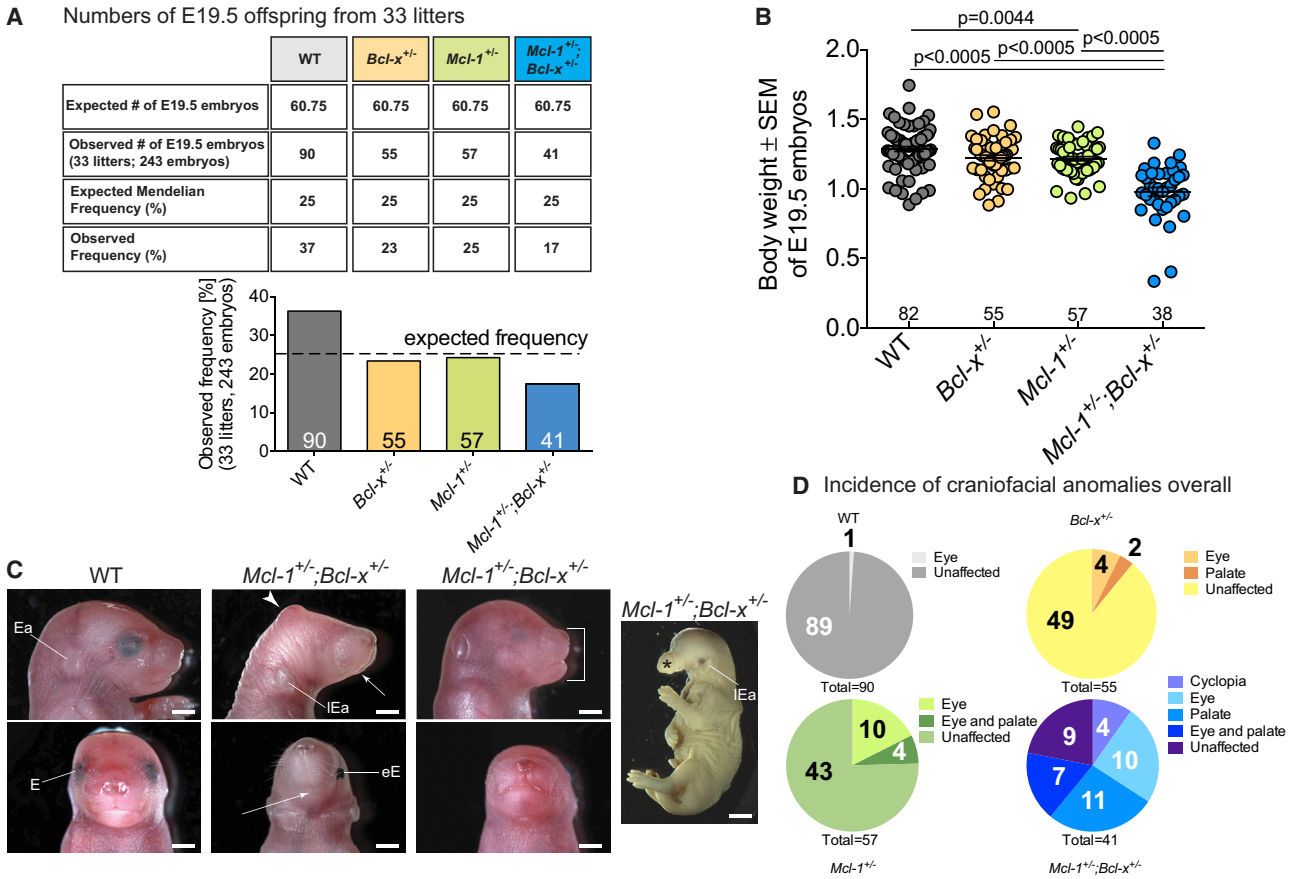

Figure 2. Craniofacial Anomalies in E19.5 *Mcl-1*$^{+/-}$;*Bcl-x*$^{+/-}$ Pups Cause Death at Birth

(A) Expected (Mendelian) and observed numbers and frequencies of E19.5 pups of the indicated genotypes from *Mcl-1*$^{+/-}$-by-*Bcl-x*$^{+/-}$ matings.

(B) Mean body weights ± SEM of E19.5 pups of the indicated genotypes.

(C) Range of craniofacial anomalies in E19.5 *Mcl-1*$^{+/-}$;*Bcl-x*$^{+/-}$ pups compared with WT controls. Scale bars, 2 mm (left six panels) and 3 mm (right).

(D) Incidence of major craniofacial anomalies in mice of the indicated genotypes.

n = number of mouse pups examined displayed in columns in (A) and (B) and pie charts in (D), as well as by individual dots in (B). E, eye, normally covered by fused eyelids at birth; Ea, ear; eE, exposed eye; lEa, low-set ear. Arrowhead, subcutaneous exencephaly; arrows, rudimentary lower jaw; bracket, shortened maxilla and mandible; asterisk, rudimentary facial structure missing nose and mouth.

each other, but neither of them with *Bcl-2*, these observations suggest a unique, gene dosage-sensitive functional overlap between MCL-1 and BCL-XL during early embryonic development.

Mcl-1$^{+/-}$;*Bcl-x*$^{+/-}$ Pups Display Gross External and Internal Cephalic Anomalies

We used serial sectioning (Figure 4A), skeletal preparations (Figure 5), and optical projection tomography (OPT) (Figure 6; Videos S1, S2, S3, and S4) to examine the cephalic structures in WT, *Mcl-1*$^{+/-}$, *Bcl-x*$^{+/-}$, and *Mcl-1*$^{+/-}$;*Bcl-x*$^{+/-}$ E19.5 pups. Serial sectioning of the heads revealed further midline defects in the *Mcl-1*$^{+/-}$;*Bcl-x*$^{+/-}$ pups, including primary and secondary palate defects, such as cleft palate and a deviated nasal septum (combined 30%). Approximately 15% of those occurred in combination with obvious eye defects (Figure 4A). Some *Mcl-1*$^{+/-}$;*Bcl-x*$^{+/-}$ pups exhibited gross underdevelopment and/or malformation of one or both eyes, and in some cases the eye was located in an abnormal medial position (Figure 4A). Additionally, *Mcl-1*$^{+/-}$;*Bcl-x*$^{+/-}$ pups displayed brain deformations and lower jaw defects; the greatest degree of severity of these defects occurred in conjunction with cyclopia (Figure 4A).

Given that we detected higher levels of *Mcl-1* mRNA in the first pharyngeal arch, and of *Bcl-x* mRNA in the first pharyngeal pouch and both *Mcl-1* and *Bcl-x* in the telencephalon (Figure 1B) (i.e., tissues that give rise to the brain, maxilla, and mandible), we hypothesized that increased apoptosis due to limiting amounts of these pro-survival proteins was responsible for the defects in craniofacial development in *Mcl-1*$^{+/-}$;*Bcl-x*$^{+/-}$ pups. Craniofacial patterning and morphogenesis commence at E8, and craniofacial structures undergo major changes between E8 and E10, such that anomalies observed at E19.5 would be expected to be present already at this earlier stage. Indeed, anomalies were already visible in E9.5 *Mcl-1*$^{+/-}$;*Bcl-x*$^{+/-}$ embryos compared with their control littermates (Figures 4B, 4C, and S1). *Mcl-1*$^{+/-}$;*Bcl-x*$^{+/-}$ E10.5 embryos (n = 8) were found to contain slightly fewer cells (Figure 4B) and were frequently smaller in

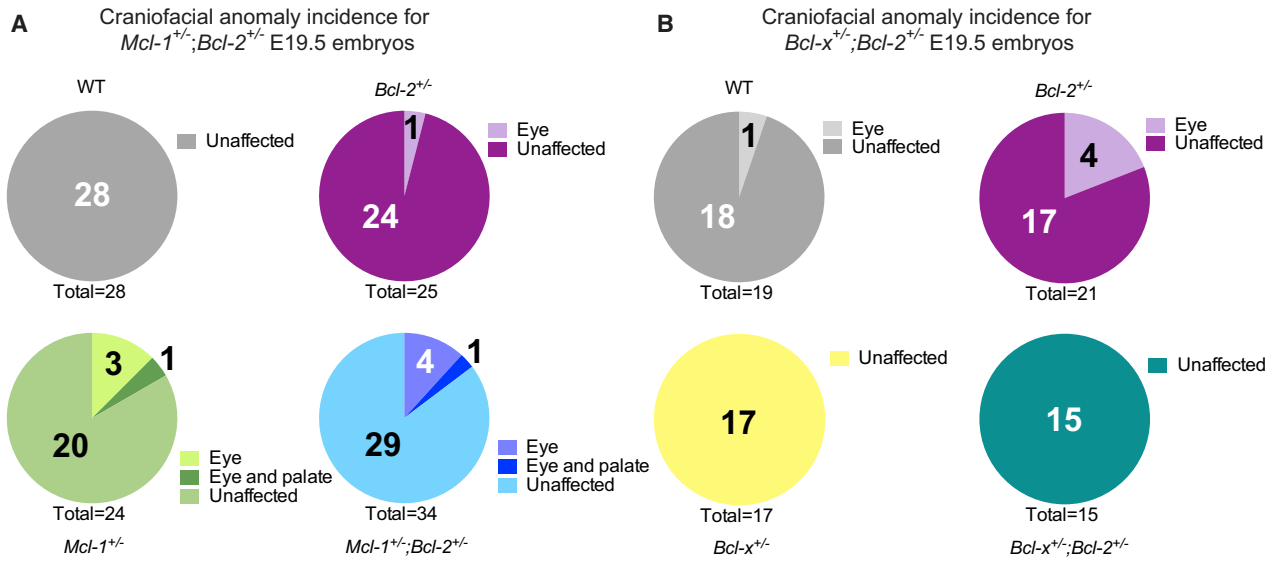

Figure 3. *Mcl-1*$^{+/-}$;*Bcl-2*$^{+/-}$ and *Bcl-x*$^{+/-}$; *Bcl-2*$^{+/-}$ Offspring Survive into Adulthood

Incidence of craniofacial anomalies for E19.5 offspring from (A) *Mcl-1*$^{+/-}$-by-*Bcl-2*$^{+/-}$ and (B) *Bcl-x*$^{+/-}$-by-*Bcl-2*$^{+/-}$ matings. n = number of mouse pups examined are displayed in the pie charts.

size compared with their littermates (Figures 4C and S1) but contained significantly more TUNEL-positive cells (i.e., cells undergoing apoptosis) compared with WT embryos (Figure 4B). Some *Mcl-1*$^{+/-}$;*Bcl-x*$^{+/-}$ embryos showed medially positioned optic vesicles and a decrease in the size of the forebrain (Figure 4C).

At E9.5 and E10.5, *Mcl-1* and *Bcl-x* mRNA are both expressed in the optic vesicle (Figure 1B). This combined with the observed anophthalmia and microphthalmia (Figures 2C and 2D and reported above) suggests that *Mcl-1*$^{+/-}$;*Bcl-x*$^{+/-}$ embryos may have abnormally increased apoptosis in the eye primordia, causing eye defects that are observed at a later stage. Three-dimensional (3D) imaging of E9.5 and E10.5 embryos demonstrated that TUNEL-positive (i.e., apoptotic) cells in *Mcl-1*$^{+/-}$;*Bcl-x*$^{+/-}$ embryos were located within similar regions as in WT, *Mcl-1*$^{+/-}$, and *Bcl-x*$^{+/-}$ embryos (Figure 4D; Videos S5 and S6). Given that the defects caused by the reduction in MCL-1 and BCL-XL were already present at E9.5, this indicates that critical structures must be insufficiently developed or lost at an earlier embryonic stage.

Compared with WT pups, the cephalic bone structures of *Mcl-1*$^{+/-}$;*Bcl-x*$^{+/-}$ pups with cyclopia showed a decrease in the size or even a loss of the intraparietal and parietal bones (4 of 10; Figure 5). Overall, the skulls of *Mcl-1*$^{+/-}$;*Bcl-x*$^{+/-}$ pups were less ossified and in some cases displayed severe structural defects (4 of 10) compared with littermates, such as a size reduction or loss of the parietal, interparietal, and supraoccipital bones, and this was associated with exencephaly (Figure 5). The mandibles were often smaller (5 of 10), missing (1 of 10), or fused in the midline (7 of 10). Almost all (9 of 10) *Mcl-1*$^{+/-}$;*Bcl-x*$^{+/-}$ pups showed palate defects. Skeletal preparations and optical projection tomography confirmed the deviation of the nasal septum observed by serial sectioning (Figure 4A) and in addition revealed anomalies or absence of the nasal and mouth cavity in *Mcl-1*$^{+/-}$;*Bcl-x*$^{+/-}$ pups (Figures 5 and 6; Videos S1, S2, S3, and S4).

In general, *Mcl-1*$^{+/-}$;*Bcl-x*$^{+/-}$ pups with less pronounced external abnormalities also displayed milder internal defects. This may suggest that in some *Mcl-1*$^{+/-}$;*Bcl-x*$^{+/-}$ embryos, the levels of MCL-1 and BCL-XL protein produced from the single intact WT alleles are almost sufficient for normal development.

Despite Morphological Similarities of the Mutant Mice, MCL-1 and BCL-XL Do Not Functionally Interact with Sonic Hedgehog Signaling

Mcl-1$^{+/-}$:*Bcl-x*$^{+/-}$ double-heterozygous pups displayed holoprosencephaly, cyclopia, and other midline development defects, similar to phenotypes observed in sonic hedgehog signaling pathway-deficient mice (Belloni et al., 1996; Chiang et al., 1996; Roessler et al., 1996). To investigate whether the similar phenotypes caused by these two distinct mutations are connected, we tested two possible functional scenarios: (1) MCL-1 and/or BCL-XL may be important for the survival of midline cells expressing the *Shh* gene, and (2) sonic hedgehog signaling may induce *Mcl1* and/or *Bclx* gene expression and/or an increase in their protein levels.

First, we generated *Mcl-1*$^{+/-}$:*Shh*$^{+/-}$ and *Bcl-x*$^{+/-}$;*Shh*$^{+/-}$ compound heterozygotes to seek evidence for a genetic interaction. *Mcl-1*$^{+/-}$;*Shh*$^{+/-}$ but not *Bcl-x*$^{+/-}$;*Shh*$^{+/-}$ double-heterozygous animals were under-represented at weaning. Among 95 animals at weaning, only 7 were *Mcl-1*$^{+/-}$;*Shh*$^{+/-}$ double heterozygotes ($p = 9 \times 10^{-6}$; Figure S2). Observation of litters suggested that the *Mcl-1*$^{+/-}$;*Shh*$^{+/-}$ pups were lost in the first week after birth. We therefore recovered litters of *Mcl-1*$^{+/-}$ by *Shh*$^{+/-}$ crosses at E18.5. Among 37 animals recovered, 9 were *Mcl-1*$^{+/-}$;*Shh*$^{+/-}$ double-heterozygous animals. One of 5 *Mcl-1*$^{+/-}$ single-heterozygous animals displayed holoprosencephaly and

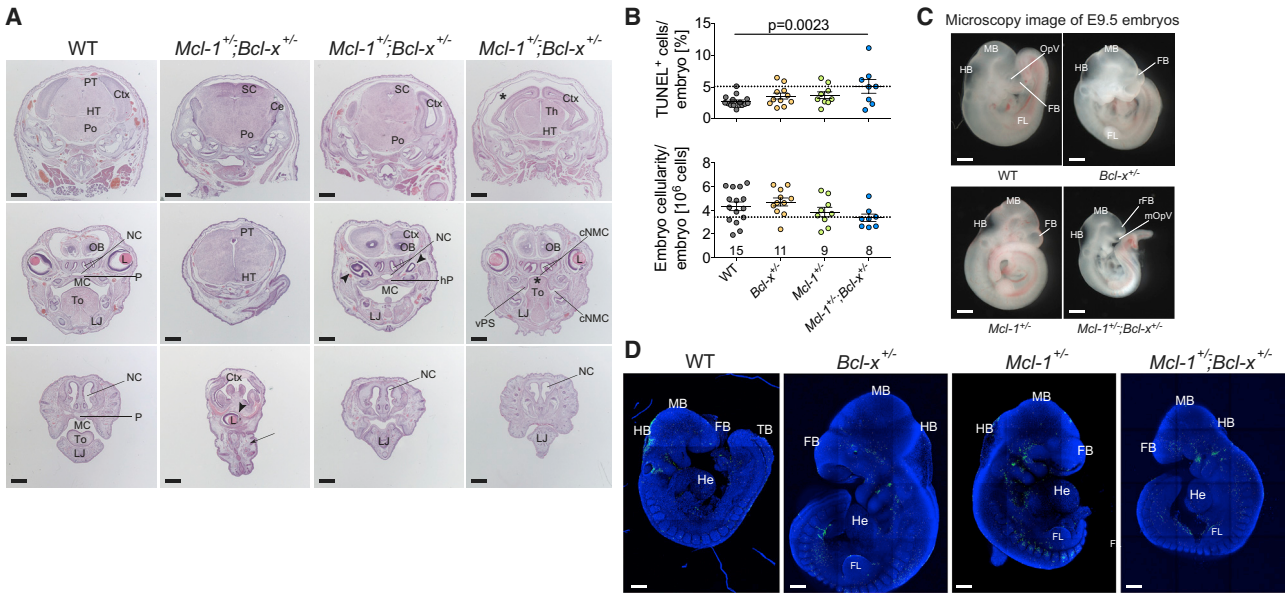

Figure 4. Developmental Defects of *Mcl-1*$^{+/-}$;*Bcl-x*$^{+/-}$ Fetuses at E19.5 and Embryos E9.5

(A) Serial coronal sections of heads from representative E19.5 *Mcl-1*$^{+/-}$;*Bcl-x*$^{+/-}$ pups compared with a WT control.

(B) Mean percentages of apoptotic cells (top) and mean total cell number (bottom) ± SEM of E9.5–E10 embryos of the indicated genotypes. n = number of mouse embryos examined displayed in each column and by individual dots.

(C) Representative examples of E9.5–E10 WT, *Mcl-1*$^{+/-}$, *Bcl-x*$^{+/-}$, and *Mcl-1*$^{+/-}$;*Bcl-x*$^{+/-}$ embryos taken at 20×.

(D) TUNEL (green) stained E9.5–E10 WT, *Mcl-1*$^{+/-}$, *Bcl-x*$^{+/-}$, and *Mcl-1*$^{+/-}$;*Bcl-x*$^{+/-}$ embryos with DAPI (blue; nucleus) counterstaining. Corresponding videos of E10.5 *Mcl-1*$^{+/-}$;*Bcl-x*$^{+/-}$ and wild-type embryos are provided in the Supplemental Information.

Ce, cerebellum; cNMC, communicating nasal and mouth cavity; Ctx, cerebral cortex; FB, forebrain; FL, forelimb bud; HB, hindbrain; He, heart; HT, hypothalamus; L, lens; LJ, lower jaw; MC, mouth cavity; MB, midbrain; mOpV; medially positioned optic vesicle; NC, nasal cavity; OB, olfactory bulb; OpV, optic vesicle; P, palate; Po, pons; PT, pretectum; rFB, rudimentary forebrain; SC, superior colliculus; Th, thalamus; To, tongue. Arrow indicates abnormal facial structure completely missing nasal and mouth cavity; arrowheads indicate abnormal eye structures; asterisk indicates tongue between vertical palatal shelves (vPS) that failed to elevate. Scale bars, 615 μm (A), 325 μm (C), and, from left to right, 165, 245, 245, and 225 μm (D). See also Figures S1–S3 and Videos S5 and S6.

a proboscis (Figure S2). The fact that defects of similar severity were not seen in *Mcl-1*$^{+/-}$ fetuses in our matings described above (Figures 1C, 2, and 3) may be due to the rarity of this event or an influence of the genetic background contributed by the *Shh*$^{+/-}$ parent. Of note, none of the 9 *Mcl-1*$^{+/-}$;*Shh*$^{+/-}$ double-heterozygous animals displayed cyclopia, holoprosencephaly, or a proboscis. Externally, all *Mcl-1*$^{+/-}$;*Shh*$^{+/-}$ double-heterozygous animals appeared normal (Figure S2).

Mcl-1$^{+/-}$;*Bcl-x*$^{+/-}$ double-heterozygous E8.5 embryos expressed *Shh* mRNA in the midline (Figure S2), similar to published results in WT embryos (Goodrich et al., 1996), showing that cells expressing the *Shh* gene can survive despite the MCL-1 and BCL-XL-reduced state.

Last, we determined if sonic hedgehog signaling induced the expression of the *Mcl-1* or *Bcl-x* genes or resulted in elevated levels of the MCL-1 or BCL-XL proteins. As a precedent, induction of *Bcl-2* gene expression by sonic hedgehog had been reported previously (Bigelow et al., 2004; Regl et al., 2004). Treatment of WT mouse embryonic fibroblasts with sonic hedgehog robustly induced expression of the known sonic hedgehog target genes *Ptch1* and *Gli1,* and the sonic hedgehog signaling pathway inhibitor vismodegib prevented this induction (Figure S3). Similarly, but to a much lesser extent, *Bcl-2* mRNA and BCL-2 protein levels were increased by sonic hedgehog treatment and reduced by vismodegib treatment (Figure S3). In contrast, sonic hedgehog and vismodegib had no impact on the mRNA or protein levels of MCL-1, BCL-XL, or pro-apoptotic BIM (Figure S3). These data indicate that a direct or indirect regulation of MCL-1 and/or BCL-XL expression by sonic hedgehog signaling and a loss of sonic hedgehog-expressing cells due to combined loss of one allele of *Bcl-x* and *Mcl-1* are not likely explanations for the similarities in the phenotypes observed between the two loss-of-function states.

Loss of One Allele of *Bim* Rescues the Craniofacial Abnormalities of *Mcl-1*$^{+/-}$;*Bcl-x*$^{+/-}$ Offspring and Their Premature Lethality

Last, we tested whether loss of a pro-apoptotic BCL-2 family member could restore normal embryonic development of *Mcl-1*$^{+/-}$;*Bcl-x*$^{+/-}$ mice. The pro-apoptotic BH3-only protein BIM can bind with high affinity to all pro-survival BCL-2 family members and is known to be critical for the initiation of apoptosis in many cell types (Bouillet et al., 1999, 2001; O'Connor et al., 1998; O'Reilly et al., 2000). Moreover, we found that *Bim* mRNA is expressed in the same regions where *Mcl-1* and *Bcl-x* mRNAs are found at higher levels (i.e., in particular the first and second pharyngeal arch and pouch and the optic and otic vesicles) (Figure 7A). Hence, we crossed *Bcl-x*$^{+/-}$ females with

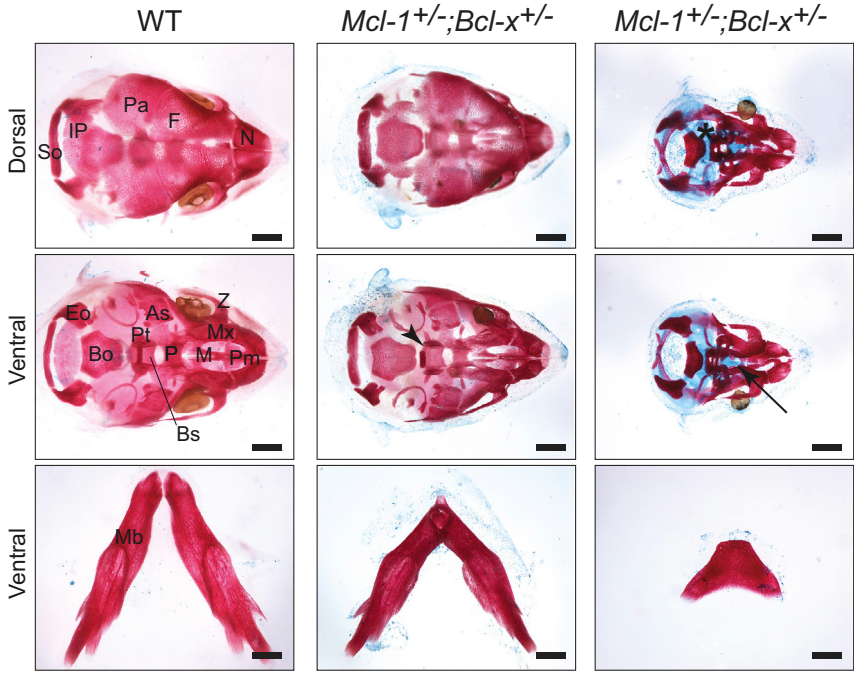

Figure 5. Skeletal Preparations of E19.5 Pups Highlighting Palatal and Skull Defects in *Mcl-1*$^{+/-}$;*Bcl-x*$^{+/-}$ Fetuses

Dorsal (top row) and ventral view (middle row) of skeletal preparations of the cranium of representative E19.5 pups of genotypes indicated after removal of the mandibles. Mandibles are taken in ventral view (bottom row). As, alisphenoid bone; Bo, basioccipital bone; Bs, basisphenoid bone; Eo, exo-occipital bone; F, frontal bone; IP, interparietal bone; M, maxillary shelf; Mb, mandible; Mx, maxilla; N, nasal bone; P, palatal shelf; Pa, parietal bone; Pm, premaxilla; Pt, pterygoid bone; So, supra-occipital bone; Z, zygomatic process. Arrow indicates where midline structures are absent; arrowhead indicates abnormal pterygoid bone allowing greater view of Bs; asterisk indicates where cranial bones are absent. Scale bar, 1.6 mm (top six panels) and 1 mm (bottom three panels).

Mcl-1$^{+/-}$;*Bim*$^{-/-}$ males. Remarkably, loss of only one allele of *Bim* was sufficient to produce healthy *Mcl-1*$^{+/-}$;*Bcl-x*$^{+/-}$;*Bim*$^{+/-}$ offspring at the expected Mendelian frequency (Figure 7B; p = 0.855). Litter sizes of *Mcl-1*$^{+/-}$;*Bim*$^{-/-}$ by *Bcl-x*$^{+/-}$ matings were similar to those of WT-by-WT intercrosses with similar proportions of pups surviving until weaning and beyond compared with littermate and WT controls (Figure 7C). Notably, these *Mcl-1*$^{+/-}$;*Bcl-x*$^{+/-}$;*Bim*$^{+/-}$ animals survived normally into adulthood without complications (n = 12; >200 days) and had a relatively normal outer appearance (Figure S4). Despite their survival advantage compared with the *Mcl-1*$^{+/-}$;*Bcl-x*$^{+/-}$ offspring, *Mcl-1*$^{+/-}$;*Bcl-x*$^{+/-}$;*Bim*$^{+/-}$ triple heterozygotes were still significantly lighter than WT animals (p = 0.0047) but not significantly different in weight from *Mcl-1*$^{+/-}$;*Bcl-x*$^{+/-}$ or *Bim*$^{+/-}$ pups (Figure 7D).

Overall, we conclude that a fine balance between pro-survival MCL-1 and BCL-XL versus pro-apoptotic BIM is critical for normal craniofacial development and survival.

DISCUSSION

Apoptosis is induced by a multitude of stress stimuli, including cytokine/growth factor withdrawal, nutrient deprivation, oncogene activation, DNA damage, chemotherapeutic drugs, and viral infection (Adams and Cory, 2007; Delbridge et al., 2016; O'Brien, 1998). Apoptosis is critical for the normal development of certain, but perhaps surprisingly not all tissues during embryogenesis (Ke et al., 2018). Apoptosis in large excess causes embryonic or fetal lethality. Of note, complete loss of MCL-1 or BCL-XL causes early or mid-gestation embryonic death in mice, respectively (Motoyama et al., 1995; Rinkenberger et al., 2000). We have shown here that developmental apoptosis needs to be finely controlled and that even loss of just one allele of *Mcl-1* and one allele of *Bcl-x* leads to a small but intolerable increase in developmental apoptosis, resulting in a very high incidence of developmental abnormalities and perinatal lethality. Because compound *Mcl-1*$^{+/-}$;*Bcl-2*$^{+/-}$ or *Bcl-x*$^{+/-}$;*Bcl-2*$^{+/-}$pups, in contrast to *Mcl-1*$^{+/-}$;*Bcl-x*$^{+/-}$ pups, displayed neither developmental abnormalities nor increased lethality compared with WT and single-heterozygous (*Mcl-1*$^{+/-}$, *Bcl-x*$^{+/-}$, or *Bcl-2*$^{+/-}$) animals, our findings reveal that only MCL-1 and BCL-XL, but not MCL-1 and BCL-2 or BCL-XL and BCL-2, have critical, overlapping roles in embryonic development.

The pro-apoptotic BH3-only protein BIM is able to bind and inhibit all pro-survival BCL-2 family members (including MCL-1 and BCL-XL) (Chen et al., 2005; Kuwana et al., 2005). Because loss of a single allele of *Bim* completely rescued the craniofacial abnormalities and premature death of *Mcl-1*$^{+/-}$;*Bcl-x*$^{+/-}$ pups, restoring normal development and even survival into late adulthood, we conclude that a surprisingly fine balance between pro-apoptotic BIM versus pro-survival MCL-1 and BCL-XL governs normal embryonic development.

MCL-1 regulation is complex, and its protein levels can drop rapidly in cells exposed to stress stimuli, because of its short half-life (Okamoto et al., 2014; Opferman, 2006). This explains why even small changes in the gene dosage of *Mcl-1* (i.e., loss of a single allele) can cause the death of both normal and malignant cells, either on its own or, more prominently, when exposed to stress stimuli (e.g., cytotoxic drugs) (Brinkmann et al., 2017; Delbridge et al., 2015; Glaser et al., 2012; Grabow et al., 2016; Kelly et al., 2014; Koss et al., 2013). Our data show that appropriate levels of MCL-1 and BCL-XL are critical for normal craniofacial development and that they are required to keep pro-apoptotic BIM in check.

Mcl-1$^{+/-}$;*Bcl-x*$^{+/-}$ double-heterozygous pups displayed holoprosencephaly, cyclopia, and other midline development defects, similar to phenotypes observed in sonic hedgehog pathway-deficient mice. Defects in signaling pathways including the sonic hedgehog and the nodal pathways, as well as

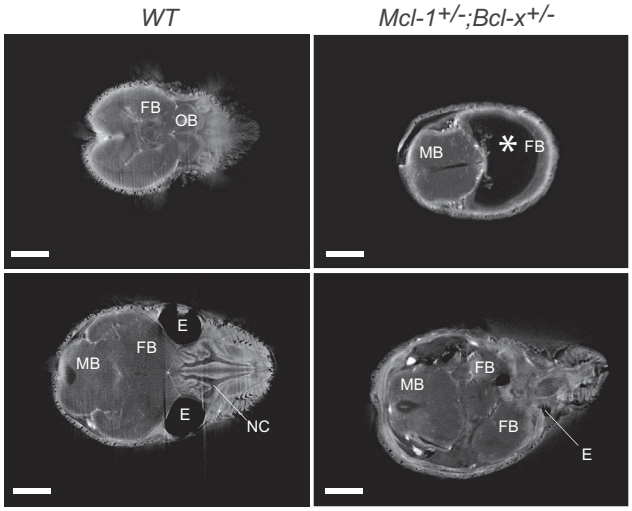

Figure 6. Optical Projection Tomography View of E19.5 WT and *Mcl-1*$^{+/-}$*;Bcl-x*$^{+/-}$ Pups

Tomographic transverse view of a WT and a *Mcl-1*$^{+/-}$*;Bcl-x*$^{+/-}$ fetus. Images were taken at the same resolution and size to highlight size differences between the fetuses. E, eye; FB, forebrain; MB, midbrain; NC, nasal cavity; OB, olfactory bulb. Asterisk indicates abnormal forebrain in the *Mcl-1*$^{+/-}$*;Bcl-x*$^{+/-}$ fetus. See also Videos S1, S2, S3, and S4 (optical projection tomography surface rendering videos and corresponding transverse sectioning videos). Scale bars, 2.2 mm.

mutations in individual genes such as *ZIC2*, *TGIF*, *SIX3*, and *SOX9*, can cause holoprosencephaly (Belloni et al., 1996; Brown et al., 1998; Chiang et al., 1996; Chu et al., 2005; Gripp et al., 2000; Nomura and Li, 1998; Roessler et al., 1996; Wallis et al., 1999; Wright et al., 1995). Cell survival in the ventral neural tube and in the neural crest, which forms the facial mesenchyme, depends critically on the presence of sonic hedgehog. Impairment of sonic hedgehog signaling due to loss of the sonic hedgehog-modifying enzyme, HHAT, was reported to lead to increased apoptosis and holoprosencephaly (Dennis et al., 2012). However, contradicting the notion that sonic hedgehog signaling might be required to restrict apoptotic cell death in the ventral neural tube, *Six3*$^{+/-}$*;Shh*$^{+/-}$ double-heterozygous embryos (the *Shh* gene is a direct target of the transcription factor SIX3) had a reduced number of apoptotic cells (Geng et al., 2008).

Interestingly, the GLI transcription factors, acting downstream of sonic hedgehog signaling, have been implicated in the regulation of the *Bcl-2* gene (Bigelow et al., 2004; Regl et al., 2004). Our data support elevation of *Bcl-2* mRNA and protein levels by sonic hedgehog signaling. However, deficiencies in BCL-2 do not appear to explain the similarities in phenotype observed between the *Mcl-1*$^{+/-}$*;Bcl-x*$^{+/-}$ double-heterozygous pups and sonic hedgehog signaling pathway mutant mice. Although *Bcl-2* gene expression is activated by sonic hedgehog in cells in culture, our results and previous findings (Bouillet et al., 2001; Veis et al., 1993) show that BCL-2 levels, at least on a WT background, are not limiting during the first half of mouse gestation. Furthermore, unlike the *Mcl-1*$^{+/-}$*;Bcl-x*$^{+/-}$ double-heterozygous pups, our *Bcl-2*$^{+/-}$*;Mcl-1*$^{+/-}$and *Bcl-2*$^{+/-}$*;Bcl-x*$^{+/-}$ compound heterozygotes did not produce an sonic hedgehog-deficiency-like phenotype.

Our genetic and biochemical studies failed to provide evidence that sonic hedgehog signaling might regulate MCL-1, BCL-XL, or BIM expression or that sonic hedgehog-expressing cells are lost when the levels of MCL-1 and BCL-XL are abnormally low (i.e., in our *Mcl-1*$^{+/-}$*Bcl-x*$^{+/-}$ embryos). On the basis of these findings, we hypothesize that sonic hedgehog signaling occurs normally in *Mcl-1*$^{+/-}$*Bcl-x*$^{+/-}$ embryos but that they retain too few cells in the critical regions for normal head midline development and that this then results in a phenocopy of the anomalies caused by deficiencies in the sonic hedgehog signaling pathway, rather than MCL-1/BCL-XL (or BIM) function and sonic hedgehog signaling being functionally linked.

Known genetic mutations explain only ~30% of holoprosencephaly (Geng and Oliver, 2009). This suggests that, along with unknown environmental causes, a number of yet to be identified genetic mutations and epigenomic alterations may cause the anomalies. Holoprosencephaly has been associated with abnormally high levels of apoptotic cell death (Aoto and Trainor, 2015; Dennis et al., 2012). The primordia of facial structures are composed of small numbers of cells that have extensive proliferative capacity. They are critical for the normal formation of structures that appear later in embryogenesis. The bilateral development and subsequent midline fusion of facial structures require precisely coordinated bilaterally symmetric development. Thus, minor reductions in the early cell number can compound over subsequent cell cycles and result in severe craniofacial anomalies that become obvious later in development. Our finding that a delicate balance between pro-survival MCL-1 and BCL-XL versus pro-apoptotic BIM is critical for normal craniofacial development may suggest that even relatively subtle changes in the levels of these regulators of apoptosis in primordial anlagen could explain some cases of developmental abnormalities in humans. Such subtle changes in MCL-1, BCL-XL, or BIM expression may arise stochastically or could be due to polymorphisms in the corresponding genes. For the latter case, one may speculate that polymorphisms in two or three of the genes, *Mcl-1*, *Bcl-x* (reduced expression), and *Bim* (increased expression) may need to collude to cause craniofacial anomalies. Future large-scale genomic analyses of affected offspring (or fetuses) and their healthy parents and siblings may provide evidence for this proposition.

A possible reason for the need to strictly control cell survival in the embryo by a finely tuned balance between pro-survival MCL-1, BCL-XL versus pro-apoptotic BIM could be that rapidly proliferating cells, such as those present during embryogenesis, are intrinsically at risk for transitioning to deregulated growth. This is exemplified by the development of teratomas (1 in 12,000–27,000 live births) as well as certain childhood cancers, particularly blastomas and leukemias (Charles, 2007). Notably, developing tissues in the embryo are provided with abundant levels of nutrients and growth factors and therefore contain large numbers of rapidly dividing cells that may through errors in DNA replication acquire oncogenic lesions. It is therefore possible that relatively facile induction of apoptosis, underpinned by significant levels of apoptosis inducers (e.g., BIM) and limiting levels of pro-survival proteins (i.e., MCL-1 and BCL-XL) is critical to safeguard developing tissues against neoplastic transformation.

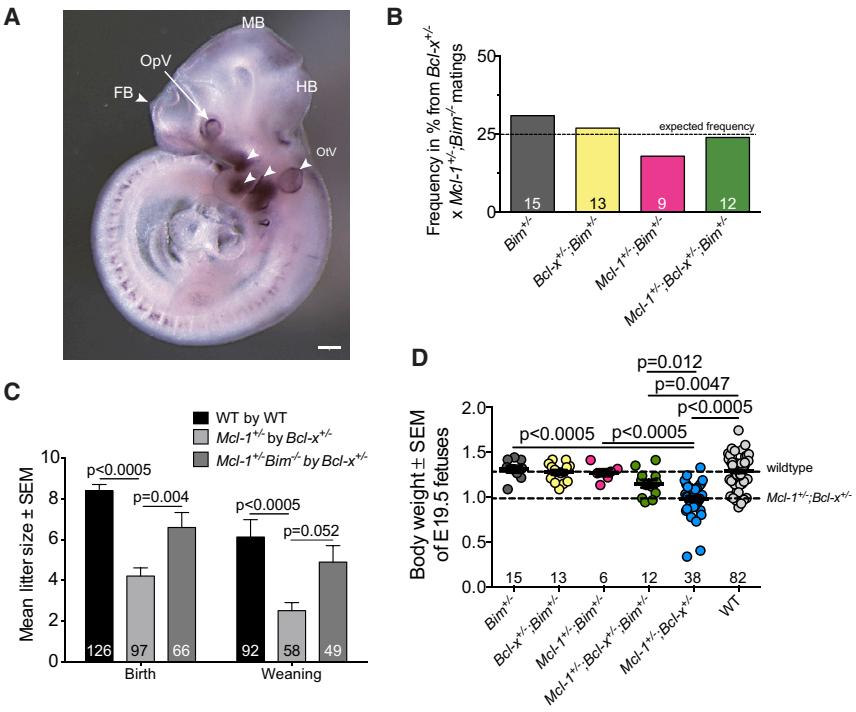

Figure 7. Loss of One Allele of *Bim* Restores Normal Development to *Mcl-1*$^{+/-}$;*Bcl-x*$^{+/-}$ Mice and Completely Prevents Their Lethality

(A) *In situ* hybridization analysis of a WT embryo to detect *Bim* mRNA. Scale bar, 135 μm.

(B) Frequency of offspring from *Bcl-x*$^{+/-}$-by-*Mcl-1*$^{+/-}$;*Bim*$^{-/-}$ matings.

(C) Mean offspring number ± SEM per litter at birth and at weaning from *Bcl-x*$^{+/-}$-by-*Mcl-1*$^{+/-}$;*Bim*$^{-/-}$ matings. The offspring numbers from WT-by-WT and *Mcl-1*$^{+/-}$-by-*Bcl-x*$^{+/-}$ matings are reproduced from Figure 1D to aid comparison.

(D) Mean body weights ± SEM of E19.5 fetuses of the indicated genotypes. Weights from WT and *Mcl-1*$^{+/-}$;*Bcl-x*$^{+/-}$ fetuses from Figure 2B are reproduced here for comparison.

n = number of mice examined displayed as numbers within bars in (B) and (C) and columns in (D), as well as individual dots in (D). See also Figure S4.

STAR★METHODS

Detailed methods are provided in the online version of this paper and include the following:

- KEY RESOURCES TABLE
- CONTACT FOR REAGENT AND RESOURCE SHARING
- EXPERIMENTAL MODEL AND SUBJECT DETAILS
  - Mice
  - Mouse embryonic fibroblasts
- METHOD DETAILS
  - Genotyping
  - Whole-mount *in situ* hybridization
  - Histology and skeletal preparation
  - Flow cytometry of TUNEL-stained cells and cell count
  - Whole-mount TUNEL staining
  - Microscopy
  - Optical Projection Tomography
  - Analysis of the Sonic Hedgehog Pathway
- QUANTIFICATION AND STATISTICAL ANALYSIS

SUPPLEMENTAL INFORMATION

Supplemental Information includes four figures, one table, and six videos and can be found with this article online at https://doi.org/10.1016/j.celrep.2018.08.048.

ACKNOWLEDGMENTS

We thank Drs. P. Bouillet, L. Hennighausen, and S.J. Korsmeyer for mice; J. Mansheim, S. O'Connor, S. Allan, C. D'Alessando, K. Landells, and G. Siciliano for expert animal care; L.A. O'Reilly for antibodies; E. Tsui, C. Tsui, V. Orlando, K. Weston, and Y. Hoang for histology services; and D. Anbarci for taking pictures of the histological slides for analysis and *in situ* preparations under the guidance of H.K.V. This work was supported by grants and fellowships from the Cancer Council of Victoria (S.G., F.K.), the Lady Tata Memorial Trust (S.G. and F.K.), the Leukaemia Foundation Australia (S.G.), the Australian Research Council (DP10310086 and Future Fellowship FT100100620 to I.M.S.), the Human Frontiers in Science Program (RGP0039/2011 to I.M.S.), the National Health and Medical Research Council (NHMRC) (Program Grant 1016701; NHMRC Fellowships 1020363 to A.S. and 575512 and 1081421 to A.K.V.; Project Grant 1051078 to A.K.V.), the Leukemia and Lymphoma Society (SCOR Grant 7001-03 to A.S.), a University of Melbourne International Research Scholarship (to S.G.), a University of Melbourne International Fee Remission Scholarship (to S.G.), an Australian Post-graduate Award (to H.K.V.), a Cancer Therapeutics CRC Top-Up Scholarship (to S.G.), and operational infrastructure grants through the Australian Government Independent Medical Research Institutes Infrastructure Support Scheme (IRIISS) and the Victorian State Government Operational Infrastructure Support (OIS) Program.

AUTHOR CONTRIBUTIONS

S.G. and A.J.K. conceived, planned, and conducted the majority of experiments. F.K. helped with ideas and planning of critical experiments and testing of new protocols. B.N.S. conducted skeletal preparations. A.J.K., H.K.V., S.E., and W.C. conducted *in situ* hybridization and recovered and examined embryos. I.M.S. and L.K.J. performed optical projection tomography experiments. M.S. and L.W. helped with imaging the embryos and computational display. M.A.D. performed gene and protein expression analysis of sonic hedgehog pathway. F.J.d.S. provided discussion and vismodegib. A.K.V. and A.S. conceived the study and provided experimental ideas and intellectual guidance. S.G., A.K.V., and A.S. wrote the manuscript.

DECLARATION OF INTERESTS

F.J.d.S. is an employee of Genentech and owns shares in Roche. A.S. serves as a consultant for Genentech. The other authors declare no competing interests.

Received: September 22, 2016
Revised: May 17, 2018
Accepted: August 16, 2018
Published: September 18, 2018

REFERENCES

Adams, J.M., and Cory, S. (2007). The Bcl-2 apoptotic switch in cancer development and therapy. Oncogene *26*, 1324–1337.

Aoto, K., and Trainor, P.A. (2015). Co-ordinated brain and craniofacial development depend upon Patched1/XIAP regulation of cell survival. Hum. Mol. Genet. *24*, 698–713.

Belloni, E., Muenke, M., Roessler, E., Traverso, G., Siegel-Bartelt, J., Frumkin, A., Mitchell, H.F., Donis-Keller, H., Helms, C., Hing, A.V., et al. (1996). Identification of Sonic hedgehog as a candidate gene responsible for holoprosencephaly. Nat. Genet. *14*, 353–356.

Bigelow, R.L., Chari, N.S., Unden, A.B., Spurgers, K.B., Lee, S., Roop, D.R., Toftgard, R., and McDonnell, T.J. (2004). Transcriptional regulation of bcl-2 mediated by the sonic hedgehog signaling pathway through gli-1. J. Biol. Chem. *279*, 1197–1205.

Bouillet, P., Metcalf, D., Huang, D.C.S., Tarlinton, D.M., Kay, T.W.H., Köntgen, F., Adams, J.M., and Strasser, A. (1999). Proapoptotic Bcl-2 relative Bim required for certain apoptotic responses, leukocyte homeostasis, and to preclude autoimmunity. Science *286*, 1735–1738.

Bouillet, P., Cory, S., Zhang, L.-C., Strasser, A., and Adams, J.M. (2001). Degenerative disorders caused by Bcl-2 deficiency prevented by loss of its BH3-only antagonist Bim. Dev. Cell *1*, 645–653.

Brinkmann, K., Grabow, S., Hyland, C.D., Teh, C.E., Alexander, W.S., Herold, M.J., and Strasser, A. (2017). The combination of reduced MCL-1 and standard chemotherapeutics is tolerable in mice. Cell Death Differ. *24*, 2032–2043.

Brown, S.A., Warburton, D., Brown, L.Y., Yu, C.Y., Roeder, E.R., Stengel-Rutkowski, S., Hennekam, R.C., and Muenke, M. (1998). Holoprosencephaly due to mutations in ZIC2, a homologue of Drosophila odd-paired. Nat. Genet. *20*, 180–183.

Carpio, M.A., Michaud, M., Zhou, W., Fisher, J.K., Walensky, L.D., and Katz, S.G. (2016). Reply to Fernandez-Marrero et al.: role of BOK at the intersection of endoplasmic reticulum stress and apoptosis regulation. Proc. Natl. Acad. Sci. U S A *113*, E494–E495.

Charles, A.K. (2007). Congenital tumors. In Fetal and Neonatal Pathology, J.W. Keeling and T.Y. Khong, eds. (Springer), pp. 327–378.

Chen, L., Willis, S.N., Wei, A., Smith, B.J., Fletcher, J.I., Hinds, M.G., Colman, P.M., Day, C.L., Adams, J.M., and Huang, D.C.S. (2005). Differential targeting of prosurvival Bcl-2 proteins by their BH3-only ligands allows complementary apoptotic function. Mol. Cell *17*, 393–403.

Chiang, C., Litingtung, Y., Lee, E., Young, K.E., Corden, J.L., Westphal, H., and Beachy, P.A. (1996). Cyclopia and defective axial patterning in mice lacking Sonic hedgehog gene function. Nature *383*, 407–413.

Chipuk, J.E., and Green, D.R. (2008). How do BCL-2 proteins induce mitochondrial outer membrane permeabilization? Trends Cell Biol. *18*, 157–164.

Chu, J., Ding, J., Jeays-Ward, K., Price, S.M., Placzek, M., and Shen, M.M. (2005). Non-cell-autonomous role for Cripto in axial midline formation during vertebrate embryogenesis. Development *132*, 5539–5551.

Combes, A.N., Short, K.M., Lefevre, J., Hamilton, N.A., Little, M.H., and Smyth, I.M. (2014). An integrated pipeline for the multidimensional analysis of branching morphogenesis. Nat. Protoc. *9*, 2859–2879.

Czabotar, P.E., Lessene, G., Strasser, A., and Adams, J.M. (2014). Control of apoptosis by the BCL-2 protein family: implications for physiology and therapy. Nat. Rev. Mol. Cell Biol. *15*, 49–63.

Delbridge, A.R., Opferman, J.T., Grabow, S., and Strasser, A. (2015). Antagonism between MCL-1 and PUMA governs stem/progenitor cell survival during hematopoietic recovery from stress. Blood *125*, 3273–3280.

Delbridge, A.R., Grabow, S., Strasser, A., and Vaux, D.L. (2016). Thirty years of BCL-2: translating cell death discoveries into novel cancer therapies. Nat. Rev. Cancer *16*, 99–109.

Dennis, J.F., Kurosaka, H., Iulianella, A., Pace, J., Thomas, N., Beckham, S., Williams, T., and Trainor, P.A. (2012). Mutations in Hedgehog acyltransferase (Hhat) perturb Hedgehog signaling, resulting in severe acrania-holoprosencephaly-agnathia craniofacial defects. PLoS Genet. *8*, e1002927.

Geng, X., and Oliver, G. (2009). Pathogenesis of holoprosencephaly. J. Clin. Invest. *119*, 1403–1413.

Geng, X., Speirs, C., Lagutin, O., Inbal, A., Liu, W., Solnica-Krezel, L., Jeong, Y., Epstein, D.J., and Oliver, G. (2008). Haploinsufficiency of Six3 fails to activate Sonic hedgehog expression in the ventral forebrain and causes holoprosencephaly. Dev. Cell *15*, 236–247.

Glaser, S.P., Lee, E.F., Trounson, E., Bouillet, P., Wei, A., Fairlie, W.D., Izon, D.J., Zuber, J., Rappaport, A.R., Herold, M.J., et al. (2012). Anti-apoptotic Mcl-1 is essential for the development and sustained growth of acute myeloid leukemia. Genes Dev. *26*, 120–125.

Goodrich, L.V., Johnson, R.L., Milenkovic, L., McMahon, J.A., and Scott, M.P. (1996). Conservation of the hedgehog/patched signaling pathway from flies to mice: induction of a mouse patched gene by Hedgehog. Genes Dev. *10*, 301–312.

Grabow, S., Delbridge, A.R., Aubrey, B.J., Vandenberg, C.J., and Strasser, A. (2016). Loss of a Single Mcl-1 Allele Inhibits MYC-Driven Lymphomagenesis by Sensitizing Pro-B Cells to Apoptosis. Cell Rep. *14*, 2337–2347.

Gripp, K.W., Wotton, D., Edwards, M.C., Roessler, E., Ades, L., Meinecke, P., Richieri-Costa, A., Zackai, E.H., Massagué, J., Muenke, M., and Elledge, S.J. (2000). Mutations in TGIF cause holoprosencephaly and link NODAL signalling to human neural axis determination. Nat. Genet. *25*, 205–208.

Harfe, B.D., Scherz, P.J., Nissim, S., Tian, H., McMahon, A.P., and Tabin, C.J. (2004). Evidence for an expansion-based temporal Shh gradient in specifying vertebrate digit identities. Cell *118*, 517–528.

Hayhurst, M., and McConnell, S.K. (2003). Mouse models of holoprosencephaly. Curr. Opin. Neurol. *16*, 135–141.

Ke, F., Voss, A., Kerr, J.B., O'Reilly, L.A., Tai, L., Echeverry, N., Bouillet, P., Strasser, A., and Kaufmann, T. (2012). BCL-2 family member BOK is widely expressed but its loss has only minimal impact in mice. Cell Death Differ. *19*, 915–925.

Ke, F.F.S., Vanyai, H.K., Cowan, A.D., Delbridge, A.R.D., Whitehead, L., Grabow, S., Czabotar, P.E., Voss, A.K., and Strasser, A. (2018). Embryogenesis and adult life in the absence of intrinsic apoptosis effectors BAX, BAK and BOK. Cell *173*, 1217–1230.e17.

Kelly, G.L., Grabow, S., Glaser, S.P., Fitzsimmons, L., Aubrey, B.J., Okamoto, T., Valente, L.J., Robati, M., Tai, L., Fairlie, W.D., et al. (2014). Targeting of MCL-1 kills MYC-driven mouse and human lymphomas even when they bear mutations in p53. Genes Dev. *28*, 58–70.

Koss, B., Morrison, J., Perciavalle, R.M., Singh, H., Rehg, J.E., Williams, R.T., and Opferman, J.T. (2013). Requirement for antiapoptotic MCL-1 in the survival of BCR-ABL B-lineage acute lymphoblastic leukemia. Blood *122*, 1587–1598.

Kulesa, P., Ellies, D.L., and Trainor, P.A. (2004). Comparative analysis of neural crest cell death, migration, and function during vertebrate embryogenesis. Dev. Dyn. *229*, 14–29.

Kuwana, T., Bouchier-Hayes, L., Chipuk, J.E., Bonzon, C., Sullivan, B.A., Green, D.R., and Newmeyer, D.D. (2005). BH3 domains of BH3-only proteins differentially regulate Bax-mediated mitochondrial membrane permeabilization both directly and indirectly. Mol. Cell *17*, 525–535.

Llambi, F., Wang, Y.M., Victor, B., Yang, M., Schneider, D.M., Gingras, S., Parsons, M.J., Zheng, J.H., Brown, S.A., Pelletier, S., et al. (2016). BOK is a non-canonical BCL-2 family effector of apoptosis regulated by ER-associated degradation. Cell *165*, 421–433.

Matsunaga, E., and Shiota, K. (1977). Holoprosencephaly in human embryos: epidemiologic studies of 150 cases. Teratology *16*, 261–272.

Motoyama, N., Wang, F., Roth, K.A., Sawa, H., Nakayama, K., Nakayama, K., Negishi, I., Senju, S., Zhang, Q., Fujii, S., et al. (1995). Massive cell death of immature hematopoietic cells and neurons in Bcl-x-deficient mice. Science *267*, 1506–1510.

Nomura, M., and Li, E. (1998). Smad2 role in mesoderm formation, left-right patterning and craniofacial development. Nature *393*, 786–790.

O'Brien, V. (1998). Viruses and apoptosis. J. Gen. Virol. *79*, 1833–1845.

O'Connor, L., Strasser, A., O'Reilly, L.A., Hausmann, G., Adams, J.M., Cory, S., and Huang, D.C.S. (1998). Bim: a novel member of the Bcl-2 family that promotes apoptosis. EMBO J. *17*, 384–395.

O'Reilly, L.A., Cullen, L., Visvader, J., Lindeman, G.J., Print, C., Bath, M.L., Huang, D.C., and Strasser, A. (2000). The proapoptotic BH3-only protein bim is expressed in hematopoietic, epithelial, neuronal, and germ cells. Am. J. Pathol. *157*, 449–461.

Okamoto, T., Coultas, L., Metcalf, D., van Delft, M.F., Glaser, S.P., Takiguchi, M., Strasser, A., Bouillet, P., Adams, J.M., and Huang, D.C. (2014). Enhanced stability of Mcl1, a prosurvival Bcl2 relative, blunts stress-induced apoptosis, causes male sterility, and promotes tumorigenesis. Proc. Natl. Acad. Sci. U S A *111*, 261–266.

Opferman, J.T. (2006). Unraveling MCL-1 degradation. Cell Death Differ. *13*, 1260–1262.

Petryk, A., Graf, D., and Marcucio, R. (2015). Holoprosencephaly: signaling interactions between the brain and the face, the environment and the genes, and the phenotypic variability in animal models and humans. Wiley Interdiscip. Rev. Dev. Biol. *4*, 17–32.

Regl, G., Kasper, M., Schnidar, H., Eichberger, T., Neill, G.W., Philpott, M.P., Esterbauer, H., Hauser-Kronberger, C., Frischauf, A.M., and Aberger, F. (2004). Activation of the BCL2 promoter in response to Hedgehog/GLI signal transduction is predominantly mediated by GLI2. Cancer Res. *64*, 7724–7731.

Rinkenberger, J.L., Horning, S., Klocke, B., Roth, K., and Korsmeyer, S.J. (2000). Mcl-1 deficiency results in peri-implantation embryonic lethality. Genes Dev. *14*, 23–27.

Roach, E., Demyer, W., Conneally, P.M., Palmer, C., and Merritt, A.D. (1975). Holoprosencephaly: birth data, benetic and demographic analyses of 30 families. Birth Defects Orig. Artic. Ser. *11*, 294–313.

Roessler, E., Belloni, E., Gaudenz, K., Jay, P., Berta, P., Scherer, S.W., Tsui, L.C., and Muenke, M. (1996). Mutations in the human Sonic Hedgehog gene cause holoprosencephaly. Nat. Genet. *14*, 357–360.

Thomas, T., Voss, A.K., Chowdhury, K., and Gruss, P. (2000). Querkopf, a MYST family histone acetyltransferase, is required for normal cerebral cortex development. Development *127*, 2537–2548.

Thomas, T., Loveland, K.L., and Voss, A.K. (2007). The genes coding for the MYST family histone acetyltransferases, Tip60 and Mof, are expressed at high levels during sperm development. Gene Expr. Patterns *7*, 657–665.

Veis, D.J., Sorenson, C.M., Shutter, J.R., and Korsmeyer, S.J. (1993). Bcl-2-deficient mice demonstrate fulminant lymphoid apoptosis, polycystic kidneys, and hypopigmented hair. Cell *75*, 229–240.

Vikstrom, I., Carotta, S., Lüthje, K., Peperzak, V., Jost, P.J., Glaser, S., Busslinger, M., Bouillet, P., Strasser, A., Nutt, S.L., and Tarlinton, D.M. (2010). Mcl-1 is essential for germinal center formation and B cell memory. Science *330*, 1095–1099.

Wagner, K.U., Claudio, E., Rucker, E.B., 3rd, Riedlinger, G., Broussard, C., Schwartzberg, P.L., Siebenlist, U., and Hennighausen, L. (2000). Conditional deletion of the Bcl-x gene from erythroid cells results in hemolytic anemia and profound splenomegaly. Development *127*, 4949–4958.

Wallis, D.E., Roessler, E., Hehr, U., Nanni, L., Wiltshire, T., Richieri-Costa, A., Gillessen-Kaesbach, G., Zackai, E.H., Rommens, J., and Muenke, M. (1999). Mutations in the homeodomain of the human SIX3 gene cause holoprosencephaly. Nat. Genet. *22*, 196–198.

Wright, E., Hargrave, M.R., Christiansen, J., Cooper, L., Kun, J., Evans, T., Gangadharan, U., Greenfield, A., and Koopman, P. (1995). The Sry-related gene Sox9 is expressed during chondrogenesis in mouse embryos. Nat. Genet. *9*, 15–20.

Youle, R.J., and Strasser, A. (2008). The BCL-2 protein family: opposing activities that mediate cell death. Nat. Rev. Mol. Cell Biol. *9*, 47–59.

STAR★METHODS

KEY RESOURCES TABLE

REAGENT or RESOURCE	SOURCE	IDENTIFIER
Antibodies		
Anti-MCL-1, rat mAB, clone 19C4	Generated in-house by Dr DCS Huang, Walter and Eliza Hall Institute of Medical research, Parkville, VIC, Australia	clone 19C4
Anti-BCL-XL, rat mAB, clone 9C9	Generated in-house by Dr LA O'Reilly, Walter and Eliza Hall Institute of Medical research, Parkville, VIC, Australia	clone 9C9
Anti-BCL-2, mouse mAB, clone 7	BD Biosciences	Cat# 610539
Anti-BIM, rabbit pAB	Enzo Life Sciences	Cat# ADI-AAP-330
Anti-HSP70, mouse mAB, clone N6	Gift from Drs R Anderson, Peter MacCallum Cancer Research Institute, Melbourne, VIC, Australia, and W Welch, University of California, San Francisco, CA, USA	clone N6
Chemicals, Peptides, and Recombinant Proteins		
Recombinant sonic hedgehog	R&D systems	Cat# 464-SH-200
Vismodegib	Genentech, in-house	N/A
Critical Commercial Assays		
In Situ Cell Death Detection Kit, TMR Red	Roche	12 156 792 910
NBT-BCIP Stock Solution	Roche	11681451001
Intracellular Fixation & Permeabilisation Buffer Set	eBioscience	88-8824-00
DIG RNA Labeling Kit (SP6/T7)	Roche	11175025910
NBT/BCIP solution	Boehringer Mannheim	1681451
Anti-Digoxigenin-AP Fab Fragments	Boehringer Mannheim	1093274
SuperScript III First Strand Synthesis SuperMix	Invitrogen	Cat# 18080400
TaqMan Gene Expression Assays	Applied Biosystems	Cat# 4369016
Experimental Models: Cell Lines		
Mouse: Mouse embryonic fibroblasts (MEFs)	This paper	N/A
Experimental Models: Organisms/Strains		
Mouse: WT C57BL/6 mice	In-house	N/A
Mouse: *Mcl-1*$^{fl/+}$ mice	Vikstrom et al., 2010	N/A
Mouse: *Bcl-x*$^{+/-}$ mice	Wagner et al., 2000	N/A
Mouse: *Bcl-2*$^{+/-}$ mice	Veis et al., 1993	N/A
Mouse: *Bim*$^{-/-}$ mice	Bouillet et al., 1999	N/A
Mouse: *Shh*$^{+/-}$ mice	Harfe et al., 2004	N/A
Oligonucleotides		
TaqMan probe: *Ptch1*	Applied Biosystems	Mm00436026_m1
TaqMan probe: *Gli1*	Applied Biosystems	Mm00494654_m1
TaqMan probe: *Mcl1*	Applied Biosystems	Mm00725832_s1
TaqMan probe: *Bcl2l1/Bclx*	Applied Biosystems	Mm00437783_m1
TaqMan probe: *Bcl2l11/Bim*	Applied Biosystems	Mm00437796_m1
TaqMan probe: *Bcl2*	Applied Biosystems	Mm00477631_m1
Mcl1 wild type allele forward primer: 5′-TCTTCTCAGGCATGCTCCGGAA-3′	Integrated DNA Technologies	N/A
Mcl1 wild type allele reverse primer: 5′-CGTCCTTACAAGAACATCTGTGA-3′	Integrated DNA Technologies	N/A

(*Continued on next page*)

Continued

REAGENT or RESOURCE	SOURCE	IDENTIFIER
Mcl1 knockout allele forward primer: 5′-CGACACAGATCAGCAGGCGTTC-3′	Integrated DNA Technologies	N/A
Mcl1 knockout allele reverse primer: 5′-TAGCCACAATCCTGTAGCCACT-3′	Integrated DNA Technologies	N/A
Bclx wild type forward primer: 5′-GAGATGCAGGTATTGGTGAGT-3′	Integrated DNA Technologies	N/A
Bclx knock out primer: 5′-TCCATTGCTCAGCGGTGCTGT-3′	Integrated DNA Technologies	N/A
Bclx common to both alleles reverse primer: 5′-GTCTCCTGAACAATCGGTATCT-3′	Integrated DNA Technologies	N/A
Bcl2 knockout forward primer: 5′-CACGAGACTAGTGAGACGTGC-3′	Integrated DNA Technologies	N/A
Bcl2 wild type forward primer: 5′-CTGAACCGGCATCTGCACACC-3′	Integrated DNA Technologies	N/A
Bcl2 reverse primer common to both alleles: 5′-CTAAAGATGCATAGGTCAAGAG-3′	Integrated DNA Technologies	N/A
Bim knockout reverse primer: 5′-CATTGCACTGAGATAGTGGTTGA-3′	Integrated DNA Technologies	N/A
Bim wild type reverse primer: 5′-CCCGTTGCACCACAGATGAA-3′	Integrated DNA Technologies	N/A
Bim forward primer common to both alleles: 5′-AAGAATCTGAGGTTGACTCTAG-3′	Integrated DNA Technologies	N/A
Cre-recombinase knockin detection in the *Shh* locus reverse primer: 5′-GCATAACCAGTGAAACAGCATTGCTG-3′	Integrated DNA Technologies	N/A
Cre-recombinase knockin detection in the *Shh* locus forward primer: 5′-GGACATGTTCAGGGATCGCCAGGCG-3′	Integrated DNA Technologies	N/A
Software and Algorithms		
Prism software	GraphPad Software	https://www.graphpad.com/
FlowJo version 10	Becton, Dickinson & Company	https://www.flowjo.com/
Stata 12.1 software	StataCorp, Texas	https://www.stata.com/

CONTACT FOR REAGENT AND RESOURCE SHARING

Further information and requests for resources and reagents should be directed to and will be fulfilled by the Lead Contact, Anne Voss (avoss@wehi.edu.au).

EXPERIMENTAL MODEL AND SUBJECT DETAILS

Mice

Experiments with mice were conducted according to the guidelines of the Walter and Eliza Hall Institute of Medical Research Animal Ethics Committee and according to the Australian code for the care and use of animals for scientific purposes. *Mcl-1*$^{+/-}$ mice were generated from *Mcl-1*$^{fl/+}$ mice (Vikstrom et al., 2010). The *Mcl-1*$^{+/-}$, *Bcl-x*$^{+/-}$ (Wagner et al., 2000), *Bcl-2*$^{+/-}$ (Veis et al., 1993), *Bim*$^{-/-}$ (Bouillet et al., 1999) and *Shh*$^{+/-}$ mice (Harfe et al., 2004) were all maintained on a C57BL/6 background. Mice were kept in a 14-hour light and 10-hour dark cycle at 22°C and fed *ad libitum*. For timed matings, noon of the day on which the vaginal plug was first observed was defined as embryonic day 0.5 (E0.5). Developmental stages of the animals are indicated in the figures and figure legends. Male and female fetuses and embryos were used randomly in the order as they were recovered. External examination and weighing of newborn mice and embryos were conducted and recorded prior to genotyping, thus blinded to the genotype of the individual animal.

Mouse embryonic fibroblasts

Mouse embryonic fibroblasts (MEFs) were isolated from WT C57BL/6 embryos, cultured on plates coated with 0.1% gelatin in DMEM with 10% FBS and used at an early passage number.

METHOD DETAILS

Genotyping

Genotyping of mice was performed using DNA samples obtained from tail biopsies, which had been digested with tail digestion buffer (Viagen Biotech, Los Angeles, CA, USA) supplemented with proteinase K (Sigma Aldrich, Castle Hill, NSW, Australia). Oligonucleotides were obtained at PCR grade from GeneWorks (Hindmarsh, SA, Australia). GoTaq Green Master Mix (Promega, Alexandria, NSW, Australia) was supplemented with 10 pmol of the appropriate oligonucleotide pairs. Oligonucleotide sequences are provided in Table S1.

Whole-mount *in situ* hybridization

Whole-mount *in situ* hybridization (WMISH) was performed as previously described (Thomas et al., 2007). In brief, paraformaldehyde-fixed embryos were dehydrated and rehydrated through methanol series. With intervening PBS/Tween 20 wash steps, embryos were treated with hydrogen peroxide, proteinase K and glycine and post-fixed in glutaraldehyde/paraformaldehyde. They were prehybridized and hybridized with *in vitro* transcribed, digoxigenin-labeled cRNA in 50% formamide/5x SSC pH4.5/1% SDS/50 μg/mL yeast RNA/50 μg/mL heparin overnight, then washed extensively, treated with RNase A, blocking reagent (Roche) and fetal bovine serum, incubated with alkaline phosphatase labeled anti-digoxigenin antibody (Roche) overnight, washed extensively and finally subjected to alkaline phosphatase reaction with NBT-BCIP (Roche) for color development. Stained embryos were washed and then cleared in glycerol.

Histology and skeletal preparation

Fetuses were fixed in Bouin's fixative and processed for paraffin embedding, serial sectioning and hematoxylin and eosin staining using standard techniques. Skeletal preparations were performed according to standard histological techniques (Thomas et al., 2000). In brief, E19.5 mouse pups were sacrificed by cooling. Skin and internal organs were removed and the remainder was fixed first 4 days in ethanol and then 4 days in acetone, prior to staining for 10 days in 0.005% (w/v) alizarin red/0.015% (w/v) alcian blue 8GX/5% (v/v) acetic acid in ethanol. Skeletal preparations were macerated for 16 days in 1% (w/v) potassium hydroxide/20% (v/v) glycerol in H_2O. Skeletons were cleared in increasing concentrations of glycerol (40, 60, 80%).

Flow cytometry of TUNEL-stained cells and cell count

Flow cytometry of TUNEL positive cells was performed as published previously (Ke et al., 2018). In brief, embryos were harvested at E10.5 and digested in trypsin. The reaction was halted by addition of 1 mL DMEM containing 10% FCS, and single cell suspensions were generated by gentle pipetting. The single cell suspension was used to count the total cell number. Cells were washed once with PBS and fixed with 2% paraformaldehyde (PFA) for 1 h at room temperature. Cells were then washed, permeabilized with 0.1% Triton-X in 0.1% sodium citrate for 2 min on ice, and, following another round of washing, TUNEL stained using the *In Situ* Cell Death Detection Kit (Roche) according to the manufacturer's instructions. Cells were counter-stained with DAPI prior to FACS analysis using the LSR IIW machine (Becton Dickinson).

Whole-mount TUNEL staining

Embryos were harvested at E9.5 and E10.5. Embryos were incubated with 1 μg/mL proteinase K (Sigma Aldrich) for 10 min at room temperature (RT), then fixed in 4% paraformaldehyde for 20 min and further incubated with 66% ethanol/33% glacial acid at −20°C for 20 min. We used the Roche *In situ* Cell Death Detection Kit, TMR red (Sigma Aldrich), following the manufacturer's instructions. Embryos were cleared for imaging by using glycerol gradients (5% to 80%) to prevent scattering and light absorption. All embryos were stained with DAPI for single cell display.

Microscopy

E9.5 and E10.5 embryos were imaged using an LSM 780 confocal microscope (Zeiss). Embryos were imaged using a 10x/0.5 NA objective at a resolution of 1024x1024 pixels using tile scanning, for movies rendered to 512x512 pixels. Z stacks were taken using 1 μm intervals and depth-correction to maintain signal strength throughout the embryo.

Optical Projection Tomography

Optical projection tomography has been previously described (Combes et al., 2014).

Analysis of the Sonic Hedgehog Pathway

For analysis of the sonic hedgehog pathway, early passage primary mouse embryonic fibroblasts (MEFs) from WT C57BL/6 embryos were seeded in 6-well plates coated with 0.1% gelatin in DMEM with 10% FBS for 24 h. Culture medium was then renewed with DMEM with 0.5% FBS. After 4 h of serum starvation, MEFs were stimulated with 0.25 or 1 μg/mL recombinant mouse Sonic Hedgehog (R&D systems) in the presence or absence of 100 nM of the Hedgehog signaling pathway inhibitor, vismodegib (Genentech), for 24 h. MEFs were then harvested for gene and protein expression analyses.

For analysis of mRNA expression, total RNA was extracted from MEFs using TRIzol reagent (Life Technologies), and cDNA was synthesized with SuperScript III First Strand Synthesis SuperMix (Invitrogen). Gene expression levels were analyzed using TaqMan Gene Expression Assays (Applied Biosystems) for *Ptch1* (Mm00436026_m1), *Gli1* (Mm00494654_m1), *Mcl1* (Mm00725832_s1), *Bcl2l1/Bclx* (Mm00437783_m1), *Bcl2l11/Bim* (Mm00437796_m1), *Bcl2* (Mm00477631_m1). *Hmbs* (Mm001143545_m1) was used for normalization of mRNA expression analysis on ViiA 7 Real-Time PCR System (Applied Biosystems). The comparative threshold cycle method was applied to determine expression levels.

For analysis of protein expression, cells were lysed using RIPA buffer and whole cell lysates in Laemmli sample buffer were electrophoresed through NuPAGE Bis-Tris gels (Invitrogen) and transferred to PVDF membrane. Blots were blocked in 5% w/v non-fat milk in TBST prior to immunoblotting. Antibodies used were rat monoclonal anti-MCL-1 clone 19C4, rat monoclonal anti-BCL-XL clone 9C9, mouse monoclonal anti-BCL-2 clone 7 (BD Biosciences Cat# 610539), rabbit polyclonal anti-BIM (Enzo Life Sciences Cat# ADI-AAP-330) and mouse monoclonal anti-HSP70 clone N6.

QUANTIFICATION AND STATISTICAL ANALYSIS

Frequencies of genotypes, body weights and developmental anomalies were plotted in GraphPad PRISM (GraphPad Software Inc, La Jolla, CA, USA). Frequencies were compared by Fisher's exact test using Stata 12.1 software (Stata Corp, Texas). Other parameters were compared by one-way ANOVA with genotype as the independent factor, where there were more than 2 experimental groups, or Student's t test, where there were only 2 experimental groups. Data are depicted as mean ± SD (Figure S3) and mean ± SEM (all other figures). Significant p values ($p < 0.05$) are displayed in each figure. N equals the number of independently performed cell culture experiments in Figure S3 and the number of mice in all other figures and is indicated in the figure legends. Male and female fetuses and embryos were used randomly in the order as recovered. External examination and weighing of newborn mice and embryos were conducted and recorded prior to genotyping, thus blinded to the genotype of the individual animal. No animal or experiment was excluded from the analyses.